Acta Astronautica 102 (2014) 89–102

Contents lists available at ScienceDirect

Acta Astronautica

journal homepage: www.elsevier.com/locate/actaastro

Magnetometer-only attitude and angular velocity filtering estimation for attitude changing spacecraft ☆

Hongliang Ma *, Shijie Xu

Department of Guidance, Navigation and Control, School of Astronautics, Beijing University of Aeronautics and Astronautics, Beijing 100191, China

ARTICLE INFO

Article history:
Received 17 September 2013
Received in revised form
29 April 2014
Accepted 4 May 2014
Available online 13 May 2014

Keywords:
Attitude and angular velocity estimation
Magnetometer-only
Improved real-time sequential filter
Observability

ABSTRACT

This paper presents an improved real-time sequential filter (IRTSF) for magnetometer-only attitude and angular velocity estimation of spacecraft during its attitude changing (including fast and large angular attitude maneuver, rapidly spinning or uncontrolled tumble). In this new magnetometer-only attitude determination technique, both attitude dynamics equation and first time derivative of measured magnetic field vector are directly leaded into filtering equations based on the traditional single vector attitude determination method of gyroless and real-time sequential filter (RTSF) of magnetometer-only attitude estimation. The process noise model of IRTSF includes attitude kinematics and dynamics equations, and its measurement model consists of magnetic field vector and its first time derivative. The observability of IRTSF for small or large angular velocity changing spacecraft is evaluated by an improved Lie-Differentiation, and the degrees of observability of IRTSF for different initial estimation errors are analyzed by the condition number and a solved covariance matrix. Numerical simulation results indicate that: (1) the attitude and angular velocity of spacecraft can be estimated with sufficient accuracy using IRTSF from magnetometer-only data; (2) compared with that of RTSF, the estimation accuracies and observability degrees of attitude and angular velocity using IRTSF from magnetometer-only data are both improved; and (3) universality: the IRTSF of magnetometer-only attitude and angular velocity estimation is observable for any different initial state estimation error vector.

1. Introduction

Miniaturization is a popular concept in the design of low-earth orbiting (LEO) spacecraft so that the attitude determination and control system with one or two kinds of sensors (such as star sensor, sun sensor, earth horizon sensor and magnetometers) become one of hot spacecraft technologies [1–5]. Among these sensors, three-axis magnetometer (TAM) is an important and essential sensor for LEO spacecraft to determine attitude and angular velocity, and implement attitude control, because of its small volume and mass, reliable performance, low power consumption and firm installation [6]. Therefore, using only TAM (TAM-only) as attitude determination sensor will be helpful for the spacecraft miniaturization development, e.g. the EduSAT microsatellite [7]. However, an all-sided TAM-only attitude determination technology requires that TAM to be a solely reliable sensor to determine the attitude of spacecraft not only in the period of steady-state (attitude) control but also in the period of attitude changing (fast and large angular attitude maneuver, rapidly spinning or uncontrolled tumble).

As for the TAM-only attitude determination method in the period of steady-state control of spacecraft, in the

☆ Foundation item: National Natural Science Foundation of China (Ref. 11272028).
* Corresponding author.
E-mail address: mahongliang317@sina.com (H. Ma).

http://dx.doi.org/10.1016/j.actaastro.2014.05.002
0094-5765/

early, the attitude, attitude rate, and constant disturbance torque estimation filter based on attitude kinematics and dynamics equations was proposed by Psiaki et al. [8]. Then, to process initial condition uncertainties and estimate three-axis attitude and attitude rate from magnetometer data, through an attitude representation of minimum quaternion, they developed a globally self-initializing attitude determination filter for steady-state control spacecraft with wire booms [9]. Also, via using a square-root unscented Kalman filter algorithm, a magnetic-only orbital and attitude estimation scheme is proposed by Cote and Lafontaine, and applied to a sun-synchronous LEO steady-state control spacecraft [10]. Hart presented a method to estimate attitude and attitude angular velocity by extended Kalman filtering and an additional single-axis Kalman filtering of state initialization for a gravity-gradient stabilized spacecraft [11]. Summarized these TAM-only attitude determination methods in the period of steady-state control of spacecraft, they can be regarded as an attitude determination method of spacecraft with only one single observation vector (TAM-only measurement vector) without angular rate measurements from gyros [12]. However, these methods for spacecraft to effectively estimate attitude and angular velocity in the period of attitude changing (fast and large angular attitude maneuver, rapidly spinning or uncontrolled tumble) have not been verified, because the measurement equation of a single observation vector only involves attitude information and is not related with attitude changing.

In the period of spacecraft attitude changing, to determine the attitude and angular velocity from TAM-only measurement data, two approaches of deterministic magnetometer-only attitude and rate determination (DADMOD) [13,14] and real-time sequential filter (RTSF) [14,15] were used successfully to obtain the attitude and angular velocity by Natanson, et al., during the earth radiation budget satellite (ERBS) experienced an on-orbit uncontrolled tumble. Then, based on TAM-only measurement data, these two methods are also used to estimate the three-axis attitude and rates of rapidly spinning gyroless spacecraft [16]. However, according to their related numerical calculation results, although the DADMOD algorithm is alike with TRIAD algorithm [17] including two dependent measurement vectors to sufficiently determine attitude, that is a magnetic field vector and its first time derivative, the TAM measurement noises in DADMOD algorithm are not processed during the attitude calculation, and because the second time derivative of magnetic field vector used in the DADMOD algorithm is in a small enough magnitude, the calculation result of angular velocity determination involves large uncertainties. Therefore, the accuracies of attitude and angular velocity determination using DADMOD algorithm are not sufficient. Compared with DADMOD algorithm, RTSF can process the measurement noises of TAM via attitude determination filtering and acquire a corrected angular velocity vector, but the attitude estimation accuracy of RTSF is also insufficient, because the angular velocity is not directly estimated via the process noise model including attitude dynamics equation and only corrected via a first-order Markov rate correction model of filter, indirectly.

Taking into account the defects of two previous TAM-only attitude determination methods for attitude changing spacecraft, an improved real-time sequential filter (IRTSF) based on RTSF, including attitude dynamics equation as a part of process noise model, is proposed to enhance the accuracies of attitude and angular velocity estimation of attitude changing spacecraft in this paper. Moreover, in order to evaluate the presented attitude determination filter, the observabilities of IRTSF for the attitude changing spacecraft with small or large initial angular velocity are evaluated by the Lie-Differentiation [18], and the degrees of observability of IRTSF for different initial estimation errors are analyzed by the condition number [19] and a solved covariance matrix [20].

The organization of this paper proceeds as follows. First, an improved attitude filter IRTSF based on TAM-only sensor, RTSF and attitude dynamics equation will be designed to estimate the attitude and angular velocity of spacecraft in the period of attitude changing. Next, observability analysis is used to evaluate the feasibility of the new TAM-only attitude determination filtering method (IRTSF). Finally, numerical simulations are implemented to verify the presented TAM-only attitude filtering method (IRTSF).

2. Mathematic modeling for improved real-time sequential filter (IRTSF)

In this section, to obtain the mathematic model of IRTSF, the process noise model and the measurement model of TAM-only attitude filtering system are, respectively, established by attitude motion equations and TAM-only measurements corresponding to the attitude changing spacecraft.

2.1. Coordinate systems

To depict the attitude changing of an on-orbit spacecraft, two coordinate frames, including the inertial reference frame $\boldsymbol{S}_i$ and the spacecraft body frame $\boldsymbol{S}_b$, are established for IRTSF. The origin of the inertial frame $\boldsymbol{S}_i$ locates at the center of mass of spacecraft, and its three axes $\boldsymbol{x}_i, \boldsymbol{y}_i$ and $\boldsymbol{z}_i$ point to the inertial space. The body frame $\boldsymbol{S}_b$ also has its origin at the center of mass of spacecraft, and its three axes $\boldsymbol{x}_b, \boldsymbol{y}_b$ and $\boldsymbol{z}_b$ point to three principle axes of spacecraft body.

If the axes order of rotation from the inertial frame $\boldsymbol{S}_i$ to the body frame $\boldsymbol{S}_b$ is chosen $3-1-2$, a set of rotation Euler angles denoted by $[\phi \quad \theta \quad \psi]^T$ respectively represents the roll, pitch and yaw angle of spacecraft relative to the inertial reference frame $\boldsymbol{S}_i$. Also, the attitude transformation matrix from the inertial frame $\boldsymbol{S}_i$ to the body frame $\boldsymbol{S}_b$ is given by

$$\boldsymbol{A}_{bi} = \boldsymbol{L}_y(\theta)\boldsymbol{L}_x(\phi)\boldsymbol{L}_z(\psi) \tag{1}$$

where the subscript *bi* represents two transformed coordinate frames and their transformation order, and $\boldsymbol{L}_x(\cdot)$, $\boldsymbol{L}_y(\cdot)$ and $\boldsymbol{L}_z(\cdot)$ are the principle rotation matrices about $\boldsymbol{x}$-, $\boldsymbol{y}$- and $\boldsymbol{z}$-axis. The transition relationship of these two frames is shown in Fig. 1. Also, in this paper, to simplify the related

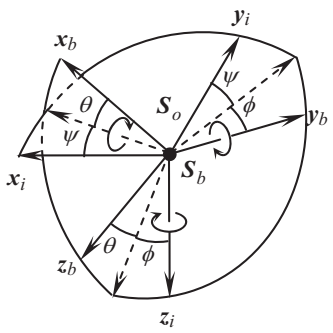

Fig. 1. Inertial reference frame and spacecraft body frame.

equation form expression of IRTSF, the measurement frame of TAM is assumed in coincidence with the body frame $\boldsymbol{S}_b$. Therefore, all measurements are denoted in the body frame $\boldsymbol{S}_b$.

2.2. Attitude motion models

If the rotation attitude quaternion from the inertial frame $\boldsymbol{S}_i$ to the body frame $\boldsymbol{S}_b$ is denoted by $\boldsymbol{q}_{bi}$ in the body frame $\boldsymbol{S}_b$, and the spacecraft angular velocity relative to the inertial coordinates is defined by $\boldsymbol{\omega}_{bi}$ in the body frame $\boldsymbol{S}_b$, the attitude kinematics equation of the body frame $\boldsymbol{S}_b$ relative to the inertial frame $\boldsymbol{S}_i$ is given by

$$\dot{\boldsymbol{q}}_{bi} = \frac{1}{2}\boldsymbol{\Omega}(\boldsymbol{\omega}_{bi})\boldsymbol{q}_{bi} \tag{2}$$

where $\boldsymbol{q}_{bi} = [q_0 \quad q_1 \quad q_2 \quad q_3]^T = [q_0 \quad \overline{\boldsymbol{q}}^T]^T$ with the scalar q_0, $\boldsymbol{\omega}_{bi} = [\omega_{bix} \quad \omega_{biy} \quad \omega_{biz}]^T$ in the body frame $\boldsymbol{S}_b$, and

$$q_0^2 + q_1^2 + q_2^2 + q_3^2 = 1 \tag{3}$$

$$\boldsymbol{\Omega}(\boldsymbol{\omega}_{ba}) = \begin{bmatrix} 0 & -\boldsymbol{\omega}_{bi}^T \\ \boldsymbol{\omega}_{bi} & -[\boldsymbol{\omega}_{bi}\times] \end{bmatrix} \tag{4}$$

$$[\boldsymbol{\omega}_{bi}\times] \equiv \begin{bmatrix} 0 & -\omega_{biz} & \omega_{biy} \\ \omega_{biz} & 0 & -\omega_{bix} \\ -\omega_{biy} & \omega_{bix} & 0 \end{bmatrix} \tag{5}$$

Here, the attitude kinematics equation of spacecraft is expressed by the attitude quaternion $\boldsymbol{q}_{bi}$ instead of the previous mentioned Euler angles, because the attitude is an inevitable large magnitude for attitude changing spacecraft, and the attitude quaternion $\boldsymbol{q}_{bi}$ can avoid the singularity that the Euler angles happen when the roll angle ϕ equals to 90 deg (°). But the advantage of the Euler angles is that the attitude represented by Euler angles is straightforward and has the physical significance as is shown in Fig. 1. Therefore, in this paper, the Euler angles are only used to depict the attitude magnitude of spacecraft, and the attitude in IRTSF is expressed by the attitude quaternion $\boldsymbol{q}_{bi}$. Via the attitude quaternion $\boldsymbol{q}_{bi}$, the attitude transformation matrix from the inertial frame $\boldsymbol{S}_i$ to the body frame $\boldsymbol{S}_b$ is given by

$$\boldsymbol{A}_{bi} = (q_0^2 - |\overline{\boldsymbol{q}}|^2)I_{3\times 3} + 2\overline{\boldsymbol{q}}\overline{\boldsymbol{q}}^T - 2q_0[\overline{\boldsymbol{q}}\times]$$

$$= \begin{bmatrix} q_0^2+q_1^2-q_2^2-q_3^2 & 2(q_1q_2+q_0q_3) & 2(q_1q_3-q_0q_2) \\ 2(q_1q_2-q_0q_3) & q_0^2-q_1^2+q_2^2-q_3^2 & 2(q_2q_3+q_0q_1) \\ 2(q_1q_3+q_0q_2) & 2(q_2q_3-q_0q_1) & q_0^2-q_1^2-q_2^2+q_3^2 \end{bmatrix} \tag{6}$$

According to Eqs. (1) and (6), the Euler angles is solved by the attitude quaternion $\boldsymbol{q}_{bi}$ as follows

$$\begin{cases} \phi = sin^{-1}[2(q_3q_2+q_1q_0)] \\ \theta = -\tan^{-1}\left[\frac{2(q_1q_3-q_2q_0)}{2(q_0^2+q_3^2)-1}\right] \\ \psi = -tan^{-1}\left[\frac{2(q_1q_2-q_0q_3)}{2(q_0^2+q_2^2)-1}\right] \end{cases} \tag{7}$$

Also, the attitude dynamics equation (Crassidis and Markley, 1997) is given by [12]

$$\dot{\boldsymbol{\omega}}_{bi} = -\boldsymbol{J}^{-1}\boldsymbol{\omega}_{bi} \times (\boldsymbol{J}\cdot\boldsymbol{\omega}_{bi} + \boldsymbol{h}) + \boldsymbol{J}^{-1}(\boldsymbol{T} - \dot{\boldsymbol{h}}) \tag{8}$$

where $\boldsymbol{J}$ is the inertia matrix of spacecraft, $\boldsymbol{h}$ is the 3×1 angular momentum vector of angular momentum device (e.g., reaction flywheels (RWs), control moment gyros (CMGs)), $\boldsymbol{T}$ is the total external torque including control torques and environmental disturbance torques. Eq. (8) involves the propagation of angular velocity, and the angular velocity vector can be determined when the angular momentum vector $\boldsymbol{h}$ and the total external torque $\boldsymbol{T}$ are known. However, these parameters cannot be obtained accurately. Therefore, via correcting the errors of these parameters, Eq. (8) is an important part for TAM-only attitude filtering system to acquire an accurate angular velocity vector, and it will be directly leaded into the process noise model of IRTSF in following section.

2.3. Process noise model

For the TAM-only attitude and angular velocity estimation filter—IRTSF, the column matrix of components of the state vector $\boldsymbol{x}$ is defined as

$$\boldsymbol{x} = \begin{bmatrix} \boldsymbol{q}_{bi}^T & \boldsymbol{\omega}_{bi}^T \end{bmatrix}^T \tag{9}$$

Then, writing matrix forms of Eqs. (2) and (8) in the body frame $\boldsymbol{S}_b$ and combining them, we can obtain the process noise model as

$$\dot{\boldsymbol{x}} = \boldsymbol{f}(\boldsymbol{x}) + D\varsigma = \begin{bmatrix} \boldsymbol{f}_1(\boldsymbol{x}) \\ \boldsymbol{f}_2(\boldsymbol{x}) \end{bmatrix} + D\varsigma \tag{10}$$

where

$$\boldsymbol{f}_1(\boldsymbol{x}) = \dot{\boldsymbol{q}}_{bi} = \frac{1}{2}\boldsymbol{q}_{bi} \otimes \boldsymbol{\omega}_{bi} \tag{11}$$

$$\boldsymbol{f}_2(\boldsymbol{x}) = \dot{\boldsymbol{\omega}}_{bi} = -\boldsymbol{J}^{-1}\boldsymbol{\omega}_{bi} \times (\boldsymbol{J}\cdot\boldsymbol{\omega}_{bi} + \boldsymbol{h}) + \mathbf{J}^{-1}(\boldsymbol{T} - \dot{\boldsymbol{h}}) \tag{12}$$

$$\mathbf{q} \otimes = \begin{bmatrix} q_0 & -q_1 & -q_2 & -q_3 \\ q_1 & q_0 & -q_3 & q_2 \\ q_2 & q_3 & q_0 & -q_1 \\ q_3 & -q_2 & q_1 & q_0 \end{bmatrix} \tag{13}$$

$$\boldsymbol{D}=\begin{bmatrix}\boldsymbol{O}_{4\times3}\\ \boldsymbol{J}^{-1}\end{bmatrix} \tag{14}$$

ς is the 3×1 parameter error vector mentioned in Eq.(8), and it is assumed to be a zero-mean Gaussian white noise vector and the corresponding variance is defined as

$$E[\varsigma(t)\varsigma(t)^T]=\mathrm{diag}([\sigma_x^2;\sigma_y^2;\sigma_z^2])\delta(t-\tau) \tag{15}$$

where σ_x, σ_y, and σ_z are the standard deviations of process angular acceleration noises, and δ denotes the Dirac delta operator. We define the spectral density matrix of process noise $\boldsymbol{e}$ as follows

$$\boldsymbol{e}=\mathrm{diag}([\sigma_x^2;\sigma_y^2;\sigma_z^2]) \tag{16}$$

Also, the discrete state propagation equation from the time step t_{k-1} to t_k is written as

$$\hat{\boldsymbol{x}}_{k/k-1}=\Xi(\hat{\boldsymbol{x}}_{k-1})=\left[\begin{array}{c}\left\{\cos\left(\frac{\sqrt{||\boldsymbol{\omega}_{bi}||}}{2}\Delta t\right)\boldsymbol{I}_{4\times4}+\ \sin\left(\frac{\sqrt{||\boldsymbol{\omega}_{bi}||}}{2}\Delta t\right)\cdot\frac{1}{\sqrt{||\boldsymbol{\omega}_{bi}||}}\cdot\begin{bmatrix}0 & -\boldsymbol{\omega}_{bi}^T\\ \boldsymbol{\omega}_{bi} & -[\boldsymbol{\omega}_{bi}\times]\end{bmatrix}\right\}\boldsymbol{q}_{bi}\\ \boldsymbol{\omega}_{bi}+\boldsymbol{f}_2(\boldsymbol{x})\Delta t+\frac{\partial}{\partial\boldsymbol{x}}\boldsymbol{f}_2(\boldsymbol{x})\boldsymbol{f}_2(\boldsymbol{x})\frac{(\Delta t)^2}{2}\end{array}\right]\Bigg|_{\substack{\boldsymbol{q}_{bi}=(\hat{\boldsymbol{q}}_{bi})_{k-1}\\ \boldsymbol{\omega}_{bi}=(\hat{\boldsymbol{\omega}}_{bi})_{k-1}}} \tag{17}$$

where the subscript "$k/k-1$" denotes the propagated estimation state at the update time, Δt is the discrete time update step of state, propagation, $\hat{\boldsymbol{q}}_{bi}$ and $\hat{\boldsymbol{\omega}}_{bi}$ represent the estimated seven states of attitude and angular velocity corresponding to the $\hat{\boldsymbol{x}}_{k-1}$, and

$$\frac{\partial}{\partial\boldsymbol{x}}\boldsymbol{f}_2(\boldsymbol{x})=\begin{bmatrix}\boldsymbol{O}_{3\times4} & -\boldsymbol{J}^{-1}\boldsymbol{F}_x+\boldsymbol{J}^{-1}[\boldsymbol{h}\times]\end{bmatrix} \tag{18}$$

$$\mathbf{F}_x=\begin{bmatrix}J_{xy}\omega_{biz}-J_{xz}\omega_{biy} & -J_{xz}\omega_{bix}+J_{yy}\omega_{biz}-2J_{yz}\omega_{biy}-J_{zz}\omega_{biz} & J_{xy}\omega_{bix}+J_{yy}\omega_{biy}+2J_{yz}\omega_{biz}-J_{zz}\omega_{biy}\\ 2J_{xz}\omega_{bix}-J_{xx}\omega_{biz}+J_{yz}\omega_{biy}+J_{zz}\omega_{biz} & J_{yz}\omega_{bix}-J_{xy}\omega_{biz} & -J_{xx}\omega_{bix}-J_{xy}\omega_{biy}+J_{zz}\omega_{bix}-2J_{xz}\omega_{biz}\\ J_{xx}\omega_{biy}-2J_{xy}\omega_{bix}-J_{yy}\omega_{biy}-J_{yz}\omega_{biz} & J_{xx}\omega_{bix}+2J_{xy}\omega_{biy}-J_{yy}\omega_{bix}+J_{xz}\omega_{biz} & J_{xz}\omega_{biy}-J_{yz}\omega_{bix}\end{bmatrix} \tag{19}$$

The state transition matrix of the process noise model (10) is written approximately as

$$\boldsymbol{\Phi}(\mathbf{x})\approx\boldsymbol{I}_{6\times6}+\Delta t\boldsymbol{F}(\mathbf{x})+\frac{1}{2}\Delta t^2\boldsymbol{F}(\boldsymbol{x})^2 \tag{20}$$

where

$$\boldsymbol{F}(\boldsymbol{x})=\begin{bmatrix}\frac{\partial}{\partial\mathbf{x}}\boldsymbol{f}_1(\boldsymbol{x})\\ \frac{\partial}{\partial\boldsymbol{x}}\boldsymbol{f}_2(\boldsymbol{x})\end{bmatrix} \tag{21}$$

$$\frac{\partial}{\partial\boldsymbol{x}}\boldsymbol{f}_1(\boldsymbol{x})=\frac{1}{2}\begin{bmatrix}0 & -\boldsymbol{\omega}_{bi}^T & -\overline{\boldsymbol{q}}^T\boldsymbol{\omega}_{bi}-[\boldsymbol{\omega}_{bi}\times]q_0\boldsymbol{I}_3+[\overline{\boldsymbol{q}}\times]\end{bmatrix} \tag{22}$$

$$[\overline{\boldsymbol{q}}\times]=\begin{bmatrix}0 & -q_3 & q_2\\ q_3 & 0 & -q_1\\ -q_2 & q_1 & 0\end{bmatrix} \tag{23}$$

2.4. Measurement model

For attitude changing spacecraft, the measurements of TAM-only includes the magnetic field vector and its first time derivative vector, and the measurement equation is given by

$$\mathbf{y}=\mathbf{h}(\mathbf{x})+\boldsymbol{\upsilon}=\begin{bmatrix}\mathbf{h}_1(\mathbf{x})\\ \mathbf{h}_2(\mathbf{x})\end{bmatrix}+\boldsymbol{\upsilon} \tag{24}$$

where $\boldsymbol{\upsilon}$ is the measurement noise vector caused by TAM sensor, and

$$\boldsymbol{h}_1(\boldsymbol{x})=\boldsymbol{b}_b=\boldsymbol{A}_{bi}\boldsymbol{b}_i \tag{25}$$

$$\boldsymbol{h}_2(\boldsymbol{x})=\dot{\boldsymbol{b}}_b=\boldsymbol{A}_{bi}\dot{\boldsymbol{b}}_i-\boldsymbol{\omega}_{bi}\times\boldsymbol{b}_b=\boldsymbol{A}_{bi}\dot{\boldsymbol{b}}_i-\boldsymbol{\omega}_{bi}\times(\boldsymbol{A}_{bi}\boldsymbol{b}_i) \tag{26}$$

where $\boldsymbol{b}_b$ is the measured magnetic field vector in the body frame $\boldsymbol{S}_b$, $\boldsymbol{b}_i$ is the magnetic field vector obtained by the orbit parameters of spacecraft (involving the absolute position and velocity vectors in inertial frame determined by the navigation system of spacecraft) and the known earth magnetic field (EMF) model (via the absolute position and velocity vectors of spacecraft to determine the latitude, longitude and magnetic field vector), e.g. 10th-order EMF model (IGRF), $\dot{\boldsymbol{b}}_b$ is the first time derivative of the measured magnetic field vector $\boldsymbol{b}_b$, and $\dot{\boldsymbol{b}}_i$ is the first time derivative of the magnetic field vector $\boldsymbol{b}_i$. The measurement equation $\boldsymbol{h}_2(\boldsymbol{x})$ in Eq. (26) includes the angular velocity information, thus, the measurements in Eq. (26) can correct the propagated angular velocity vector in Eq. (8), directly. And it is the reason that Eq. (8) is leaded into the process noise model to effectively estimate the angular velocity. Note: the orbit determination parameters of spacecraft are considered known to analyze the algorithm of attitude determination.

The column matrix of measurement noise vector $\boldsymbol{\upsilon}$ is written as

$$\boldsymbol{\upsilon} = \begin{bmatrix} \upsilon_{bx} & \upsilon_{by} & \upsilon_{bz} & \upsilon_{\Delta bx} & \upsilon_{\Delta by} & \upsilon_{\Delta bz} \end{bmatrix}^T \tag{27}$$

These measurement noises are assumed to be white Gaussian noises. We define the covariance matrix $\boldsymbol{R}$ of measurement uncertainty as

$$E[\boldsymbol{\nu}(t)\boldsymbol{\nu}(t)^T] = \boldsymbol{R}\delta(t-\tau) \tag{28}$$

$$\mathbf{R} = \mathrm{diag}([\sigma_{bx}^2; \sigma_{by}^2; \sigma_{bz}^2; \sigma_{\Delta bx}^2; \sigma_{\Delta by}^2; \sigma_{\Delta bz}^2]) \tag{29}$$

where the covariance matrix $\boldsymbol{R}$ of measurement uncertainty is a 6×6 constant main diagonal matrix, and the σ_{bx}, σ_{by}, σ_{bz}, $\sigma_{\Delta bx}$, $\sigma_{\Delta by}$ and $\sigma_{\Delta bz}$ are standard deviations of measurement noises, respectively. In this paper, the σ_{bx}, σ_{by} and σ_{bz} are assumed to satisfy $\sigma_{bx}=\sigma_{by}=\sigma_{bz}$, the $\sigma_{\Delta bx}$, $\sigma_{\Delta by}$ and $\sigma_{\Delta bz}$ are assumed to satisfy $\sigma_{\Delta bx}=\sigma_{\Delta by}=\sigma_{\Delta bz}$, and the relations between σ_{bx} and $\sigma_{\Delta bx}$ is approximately given by

$$\sigma_{\Delta bx} \approx \frac{2\sigma_{bx}}{\Delta T} \tag{30}$$

where ΔT is the measurement updating period of TAM.

Obviously, the measurement functions in Eq. (24) are nonlinear, so we require the measurement sensitivity matrix of system as follows

$$\boldsymbol{H}(\boldsymbol{x}) = \begin{bmatrix} \frac{\partial}{\partial \boldsymbol{x}}\boldsymbol{h}_1(\boldsymbol{x}) \\ \frac{\partial}{\partial \boldsymbol{x}}\boldsymbol{h}_2(\boldsymbol{x}) \end{bmatrix} \tag{31}$$

where

$$\frac{\partial}{\partial \boldsymbol{x}}\boldsymbol{h}_1(\boldsymbol{x}) = 2\begin{bmatrix} \boldsymbol{H}_{11}\boldsymbol{b}_i & \mathbf{H}_{12}\mathbf{b}_i & \boldsymbol{H}_{13}\boldsymbol{b}_i & \boldsymbol{H}_{14}\boldsymbol{b}_i & \boldsymbol{O}_{3\times 3} \end{bmatrix} \tag{32}$$

$$\begin{aligned} \frac{\partial}{\partial \mathbf{x}}\ \mathbf{h}_2(\mathbf{x}) = 2\big[& \mathbf{H}_{21}\dot{\mathbf{b}}_i - [\boldsymbol{\omega}_{bi}\times]\mathbf{H}_{21}\mathbf{b}_i \\ & \mathbf{H}_{22}\dot{\mathbf{b}}_i - [\boldsymbol{\omega}_{bi}\times]\mathbf{H}_{22}\mathbf{b}_i \\ & \mathbf{H}_{23}\dot{\mathbf{b}}_i - [\boldsymbol{\omega}_{bi}\times]\mathbf{H}_{23}\mathbf{b}_i \\ & \mathbf{H}_{24}\dot{\mathbf{b}}_i - [\boldsymbol{\omega}_{bi}\times]\mathbf{H}_{24}\mathbf{b}_i \frac{1}{2}[(\mathbf{A}_{bi}\mathbf{b}_i)\times]\big] \end{aligned} \tag{33}$$

$$\mathbf{H}_{21} = \begin{bmatrix} q_0 & q_3 & -q_2 \\ -q_3 & q_0 & q_1 \\ q_2 & -q_1 & q_0 \end{bmatrix} \tag{34}$$

$$\mathbf{H}_{22} = \begin{bmatrix} q_1 & q_2 & q_3 \\ q_2 & -q_1 & q_0 \\ q_3 & -q_0 & -q_1 \end{bmatrix} \tag{35}$$

$$\mathbf{H}_{23} = \begin{bmatrix} -q_2 & q_1 & -q_0 \\ q_1 & q_2 & q_3 \\ q_0 & q_3 & -q_2 \end{bmatrix} \tag{36}$$

$$\mathbf{H}_{24} = \begin{bmatrix} -q_3 & q_0 & q_1 \\ -q_0 & -q_3 & q_2 \\ q_1 & q_2 & q_3 \end{bmatrix} \tag{37}$$

2.5. Extended Kalman filtering

The Kalman filter is an optimal estimator for linear systems. But many dynamic systems and measurement sensors are not absolutely linear. Therefore, an extension of the Kalman filter, named extended Kalman filter (EKF), is developed for nonlinear systems [21,22]. The EKF, working by linearizing the nonlinear dynamics and measurements, is not an optimal estimator but a suboptimal estimator for nonlinear systems. The more complete description and analysis of the EKF are introduced in references by Gelb [22] and Crassidis and Junkins [23].

Based on the process noise model Eq. (10) and the measurement model Eq. (24) of the IRTSF, a discrete-time EKF is designed to estimate the attitude angle and angular velocity as follows

$$\hat{\boldsymbol{x}}_{k/k-1} = \boldsymbol{\Xi}(\hat{\boldsymbol{x}}_{k-1}) \tag{38}$$

$$\hat{\boldsymbol{x}}_k = \hat{\boldsymbol{x}}_{k/k-1} + \boldsymbol{K}_k\left[\hat{\boldsymbol{y}}_k - \boldsymbol{h}(\hat{\boldsymbol{x}}_{k/k-1})\right] \tag{39}$$

$$\mathbf{K}_k = \mathbf{P}_{k/k-1}\mathbf{H}_k^T\left(\mathbf{H}_k\mathbf{P}_{k/k-1}\mathbf{H}_k^T + \mathbf{R}_k\right)^{-1} \tag{40}$$

$$\boldsymbol{P}_{k/k-1} = \boldsymbol{\Phi}_{k,k-1}\boldsymbol{P}_{k-1}\boldsymbol{\Phi}_{k,k-1}^T + \mathbf{Q}_{k-1} \tag{41}$$

$$\boldsymbol{P}_k = (\boldsymbol{I} - \boldsymbol{K}_k\boldsymbol{H}_k)\boldsymbol{P}_{k/k-1}(\boldsymbol{I} - \boldsymbol{K}_k\boldsymbol{H}_k)^T + \boldsymbol{K}_k\boldsymbol{R}_k\boldsymbol{K}_k^T \tag{42}$$

where

$$\boldsymbol{\Phi}_{k,k-1} = \boldsymbol{\Phi}(\hat{\mathbf{x}}_{k-1}), \boldsymbol{H}_k = \boldsymbol{H}\left(\hat{\boldsymbol{x}}_{k/k-1}\right), \quad \boldsymbol{R}_k = \boldsymbol{R} \tag{43}$$

$\boldsymbol{P}$ is the 7×7 covariance matrix of state estimation uncertainty. The covariance matrix of the discrete-time process noise $\boldsymbol{Q}_k$ is calculated by [24]

$$\boldsymbol{Q}_k = \int_{t_{k-1}}^{t_k} \boldsymbol{\Phi}_{k,k-1}\boldsymbol{D}\boldsymbol{q}\boldsymbol{D}^T\boldsymbol{\Phi}_{k,k-1}^T dt \tag{44}$$

3. Observability of IRTSF

Investigating the observability of a new filtering system is important because it is a way to evaluate the feasibility of the system such that the states of the system can be reliably estimated from the measurements. In this section, an improved Lie-Differentiation, the condition number and a solved covariance matrix to evaluate the observability of the IRTSF are introduced. The first method is used to determine the observability of the IRTSF via solving the observability matrix rank of the filtering system. The latter two methods are mainly used to acquire and compare the observability degrees of the IRTSF and the RTSF.

3.1. Lie-Differentiation

The conception of locally weak observability of nonlinear system has been given by Hermann [18]. In his theory of the local weak observability, if a deterministic nonlinear systemic function is followed by

$$\Sigma\begin{cases} \dot{\boldsymbol{x}} = \boldsymbol{f}(\boldsymbol{x}) \\ \boldsymbol{y} = \boldsymbol{h}(\boldsymbol{x}) \end{cases} \tag{45}$$

where $\boldsymbol{x}$ is a n-dimension state vector and belongs to the definition region $\boldsymbol{U}$, $\boldsymbol{f}$ is the state function of nonlinear system, $\boldsymbol{y}$ is the measurement vector, and $\boldsymbol{h}$ is the measurement function of nonlinear system, the observability matrix of system Σ is given by

$$\boldsymbol{M}=\begin{bmatrix} d\boldsymbol{L}_{\mathbf{f}}^{0}\boldsymbol{h}(\boldsymbol{x}) \\ d\boldsymbol{L}_{\mathbf{f}}^{1}\boldsymbol{h}(\boldsymbol{x}) \\ \vdots \\ d\boldsymbol{L}_{\mathbf{f}}^{n-1}\boldsymbol{h}(\boldsymbol{x}) \end{bmatrix} \tag{46}$$

where $d\boldsymbol{L}_{\mathbf{f}}^{i}\boldsymbol{h}(\boldsymbol{x})$ is the ith order Li-Differentiation and

$$d\boldsymbol{L}_{\mathbf{f}}^{0}\boldsymbol{h}(\boldsymbol{x})=\boldsymbol{h}(\boldsymbol{x}) \tag{47}$$

$$\boldsymbol{L}_{\mathbf{f}}^{i}\boldsymbol{h}(\boldsymbol{x})=\frac{\partial(\boldsymbol{L}_{\mathbf{f}}^{i-1}\boldsymbol{h})}{\partial\boldsymbol{x}}\boldsymbol{f}(\mathbf{x}),\quad i=1,2,\ldots,n-1 \tag{48}$$

$$d\boldsymbol{L}_{\mathbf{f}}^{i}\boldsymbol{h}(\boldsymbol{x})=\frac{\partial(\boldsymbol{L}_{\mathbf{f}}^{i}\boldsymbol{h})}{\partial\boldsymbol{x}}\quad i=1,2,\ldots,n-1 \tag{49}$$

Lemma 1. *For any state vector $\boldsymbol{x}$ in the definition region $\boldsymbol{U}$, if the rank of observability matrix $\boldsymbol{M}$ satisfies* $\mathrm{rank}(\boldsymbol{M}(\boldsymbol{x}))=n$, *the system Σ is locally weakly observable, or the system Σ is unobservable.*

The proof of Lemma 1 has been given by Hermann [18]. However, although the locally weak observability of any nonlinear filtering system can be judged by Lemma 1, due to the complex calculation relations of the parameters in the nonlinear Eq. (45), the observability matrix $\mathbf{M}$ is difficult or impossible to be calculated for the higher order Li- Differentiation, that is a large i. Therefore, an important corollary of Lemma 1 is given to evaluate the locally weak observability of IRTSF in the following content.

For Eq. (46), the observability matrix $\boldsymbol{M}$ can also be written as

$$\boldsymbol{M}=\begin{bmatrix} d\boldsymbol{L}_{\mathbf{f}}^{0}\boldsymbol{h}(\boldsymbol{x}) \\ \vdots \\ d\boldsymbol{L}_{\mathbf{f}}^{l-1}\boldsymbol{h}(\boldsymbol{x}) \\ \hline d\boldsymbol{L}_{\mathbf{f}}^{l}\mathbf{h}(\mathbf{x}) \\ \vdots \\ d\boldsymbol{L}_{\mathbf{f}}^{n-1}\mathbf{h}(\mathbf{x}) \end{bmatrix},\quad l\in[1,n]\quad\text{and}\quad lm\geq n \tag{50}$$

Therefore, a low dimension observability matrix $\boldsymbol{M}_l$ for any integer l is given by

$$\mathbf{M}_{l}=\begin{bmatrix} d\mathbf{L}_{\mathbf{f}}^{0}\mathbf{h}(\mathbf{x}) \\ d\mathbf{L}_{\mathbf{f}}^{1}\mathbf{h}(\mathbf{x}) \\ \vdots \\ d\mathbf{L}_{\mathbf{f}}^{l-1}\mathbf{h}(\mathbf{x}) \end{bmatrix},\quad l\in[1,n]\quad\text{and}\quad lm\geq n \tag{51}$$

Corollary of Lemma 1: the system Σ in Eq. (45) is also locally weakly observable if, the rank of the observability matrix $\boldsymbol{M}_l$ satisfies

$$\mathrm{Rank}(\boldsymbol{M}_{l}(\mathbf{x}))=n \tag{52}$$

where m is the dimension of measurement vector.

Proof. The observability matrix of the system Σ in Eq. (45) has been given by Eq. (50). Obviously, the rank of the observability matrix $\boldsymbol{M}$ satisfies

$$n\geq\mathrm{rank}(\boldsymbol{M}(\boldsymbol{x}))\geq\mathrm{rank}(\boldsymbol{M}_{l}(\boldsymbol{x})) \tag{53}$$

According to Eq. (51), if $\mathrm{rank}(\boldsymbol{M}_l(\boldsymbol{x}))=n$, the rank of observability matrix $\boldsymbol{M}$ for the system Σ in Eq. (45) satisfies

$$n\geq\mathrm{rank}(\boldsymbol{M}(\boldsymbol{x}))\geq\mathrm{rank}(\boldsymbol{M}_{l}(\boldsymbol{x}))=n\Rightarrow\mathrm{rank}(\boldsymbol{M}(\boldsymbol{x}))=n \tag{54}$$

Therefore, the system Σ is locally weakly observable via Lemma 1.

Obviously, for the IRTSF with the 7×1 dimension state vector and the 6×1 dimension measurement vector, the minimum parameter l in Eq. (51) can take 2, which will make the calculation of the observability matrix $\boldsymbol{M}_l$ possible and easy. Also, to evaluate a new filtering system IRTSF, if it is locally weak observable via the Li-Differentiation in Eq. (51), we still need to acquire the degree of its observability. The degree of the observability of the IRTSF will be obtained by the following condition number and a solved covariance matrix. As a result, the universality of the nonlinear filtering system IRTSF can be determined.

3.2. Condition number and solved covariance matrix

For the deterministic nonlinear systemic function in Eq.(45), its discrete linearized equation is given by

$$\begin{cases}\delta\boldsymbol{x}_{k}=\boldsymbol{\Phi}\delta\boldsymbol{x}_{k-1}\\ \delta\boldsymbol{y}_{k}=\boldsymbol{H}\delta\boldsymbol{x}_{k}\end{cases} \tag{55}$$

where $\boldsymbol{\Phi}$ and $\boldsymbol{H}$ are those forms as described in Eqs. (20) and (31) for the IRTSF in this paper.

For the discrete system equation in Eq. (55), if the true initial state, the nominal initial state and the initial estimation state are respectively denoted by $\boldsymbol{x}_0$, $\bar{\boldsymbol{x}}_0$ and $\hat{\boldsymbol{x}}_0$, the initial state estimation error is denoted by $\delta\mathbf{x}_0$, and the estimation error covariance matrix is denoted by $\boldsymbol{P}_0$, after the kth measurement $\boldsymbol{y}_i$ (Fig. 2), the minimized cost function $\boldsymbol{J}_e$ can be given by the following error quadratic form

$$\begin{aligned}\boldsymbol{J}_{e}=&(\delta\bar{\mathbf{x}}_{0}-\delta\mathbf{x}_{0})^{T}\boldsymbol{P}_{0}^{-1}(\delta\bar{\mathbf{x}}_{0}-\delta\mathbf{x}_{0})\\&+\sum_{i=0}^{k}\left(\delta\boldsymbol{y}_{i}-\boldsymbol{H}_{i}\delta\boldsymbol{x}_{i}\right)^{T}\boldsymbol{R}_{i}^{-1}\left(\delta\boldsymbol{y}_{i}-\boldsymbol{H}_{i}\delta\boldsymbol{x}_{i}\right)\end{aligned} \tag{56}$$

where $\delta\bar{\boldsymbol{x}}_0$ is the mean error for a set of initial random state error, $\boldsymbol{P}_0$ is taken as a weighted matrix, $\delta\boldsymbol{x}_i$ is the ith state estimation error and propagated by Eq. (55), $\delta\boldsymbol{y}_i$ is the ith

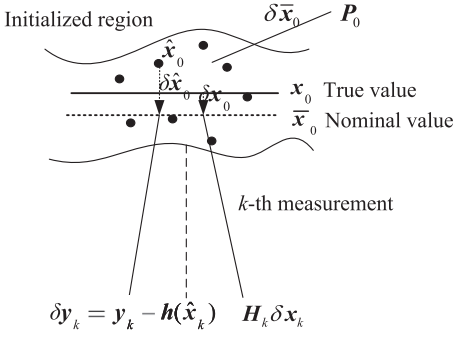

Fig. 2. Propagation of discrete linearized system.

measurement error and obtained via the ith measurement subtracting the estimated measurement in Eq. (45), $\boldsymbol{R}_i$ is the covariance matrix of measurement uncertainty (such as the measurement error caused by TAM for the IRTSF in the paper) and also a weighted matrix. The measurement difference equation is given by

$$\begin{bmatrix} \delta \boldsymbol{y}_0 \\ \delta \boldsymbol{y}_1 \\ \delta \boldsymbol{y}_2 \\ \vdots \\ \delta \boldsymbol{y}_k \end{bmatrix} = \begin{bmatrix} \boldsymbol{H}_0 \\ \boldsymbol{H}_1 \boldsymbol{\Phi}_{1/0} \\ \boldsymbol{H}_2 \boldsymbol{\Phi}_{2/0} \\ \vdots \\ \boldsymbol{H}_k \boldsymbol{\Phi}_{k/0} \end{bmatrix} \delta \boldsymbol{x}_0 \tag{57}$$

where $\boldsymbol{\Phi}_{k/0}$ represents the transition matrix of the initial state estimation error from the 0th state to the kth state, and $\boldsymbol{\Phi}_{k/0}$ can be approximately solved by

$$\boldsymbol{\Phi}_{k/0} \approx \boldsymbol{\Phi}_0 \cdot \boldsymbol{\Phi}_1 \cdots \boldsymbol{\Phi}_{k-1} \cdot \boldsymbol{\Phi}_k \tag{58}$$

The observability matrix of the nonlinear system in Eq. (45) is defined as following:

$$\boldsymbol{M}_{0/k} = \sum_{i=0}^{k} \boldsymbol{\Phi}_{i/0}^T \boldsymbol{H}_i^T \boldsymbol{R}_i^{-1} \boldsymbol{H}_i \boldsymbol{\Phi}_{i/0} \tag{59}$$

Therefore, after the kth measurement, the corrected initial state estimation error $\delta \boldsymbol{x}_{k/0}$ is given by the weighted least squares method as follows

$$\frac{\partial \boldsymbol{J}_e}{\partial(\delta \boldsymbol{x}_0)} = 0 \Rightarrow \delta \hat{\boldsymbol{x}}_{0/k} = (P_0^{-1} + \boldsymbol{M}_{0/k})^{-1} (\boldsymbol{Z}_{0/k} + \boldsymbol{P}_0^{-1} \delta \overline{\boldsymbol{x}}_0) \times (\boldsymbol{I}_7 + \boldsymbol{P}_0 \boldsymbol{M}_{0/k})^{-1} (\boldsymbol{P}_0 \boldsymbol{Z}_{0/k} + \delta \overline{\boldsymbol{x}}_0) \tag{60}$$

$$\boldsymbol{Z}_{0/k} = \sum_{i=0}^{k} \boldsymbol{\Phi}_{i/0}^T \boldsymbol{H}_i^T \boldsymbol{R}_i^{-1} \delta \boldsymbol{y}_i \tag{61}$$

Also, the covariance matrix $\boldsymbol{P}_{0/k}$ of the corrected initial state estimation error is calculated by

$$\boldsymbol{P}_{0/k} = E\left[(\delta \hat{\boldsymbol{x}}_{0/k} - \delta \boldsymbol{x}_0)(\delta \hat{\boldsymbol{x}}_{0/k} - \delta \boldsymbol{x}_0)^T \right] \tag{62}$$

$$(\boldsymbol{P}_0 - \boldsymbol{P}_{0/k}) \boldsymbol{P}_0^{-1} = \boldsymbol{P}_{0/k} \boldsymbol{M}_{0/k} \tag{63}$$

The null spaces of $\boldsymbol{M}_{0/k}$ and $(\boldsymbol{P}_0 - \boldsymbol{P}_{0/k})$ are different according to Eq. (63), but they can be both used to analyze the observability degree of nonlinear system.

For the observability matrix $\boldsymbol{M}_{0/k}$, its condition number can be utilized to analyze the observability degree of the nonlinear system. The condition number that is the ratio of the singular values of the observability matrix can be obtained by dividing the largest singular value by the smallest singular value [19]. $\boldsymbol{M}_{0/k}$ is a symmetric and nonnegative matrix, and the largest singular $\sigma_{\max}$ and the smallest singular $\sigma_{\min}$ can be solved by the singular value decomposition (SVD) of $\boldsymbol{M}_{0/k}$. Therefore, the condition number $cond(\boldsymbol{M}_{0/k})$ of the observability matrix $\boldsymbol{M}_{0/k}$ is given by

$$Cond(\boldsymbol{M}_{0/k}) = \frac{\sigma_{\max}}{\sigma_{\min}} \tag{64}$$

If the condition number is small, the difference between the smallest singular $\sigma_{\min}$ and the largest singular $\sigma_{\max}$ is small. For a large enough $\sigma_{\min}$, the measurement vector of the nonlinear system in Eq. (45) is insensitive to the external perturbation, and the observability degree of the system is high.

For the difference matrix $\boldsymbol{P}_0 - \boldsymbol{P}_{0/k}$ between the initial covariance matrix $\boldsymbol{P}_0$ and the covariance matrix of the corrected initial state estimation error $\boldsymbol{P}_{0/k}$, a theorem [20] to evaluate the observability of linear system is given as follows:

Lemma 2. *For a vector $\boldsymbol{u}$ in the unobservable subspace, if $\boldsymbol{U}_{ko}^T \boldsymbol{P}_0 \boldsymbol{u} \neq 0$, then $\boldsymbol{u}(\boldsymbol{P}_0 - \boldsymbol{P}_{0/k})\boldsymbol{u}^T > 0$.*

where $\boldsymbol{U}_{ko}$ is the singular vector matrix corresponding to the positive singular values of the SVD of $\boldsymbol{M}_{0/k}$.

The theorem states that the initial state estimation covariance in the direction of some unobservable vector can decrease depending on the measurements of system, and the vector $\boldsymbol{u}$ in the unobservable subspace is considered locally weakly observable. Therefore, another method in this paper to analyze the observability of a specific state is given as follows

Corollary 1 of Lemma 2. *$(\boldsymbol{P}_0^{-1}\boldsymbol{u})(\boldsymbol{P}_0 - \boldsymbol{P}_{0/k})(\boldsymbol{P}_0^{-1}\boldsymbol{u})^T > 0 \Rightarrow \boldsymbol{u}$ is locally weakly observable, or $\boldsymbol{u}$ is unobservable (do not need to be proved).*

And, in this paper, the observability degree of the nonlinear system in Eq. (45) can also be evaluated by

$$\zeta_k = \frac{(\boldsymbol{P}_0)_{ij} - (\boldsymbol{P}_{0/k})_{ij}}{(\boldsymbol{P}_0)_{ij}} \times 100\%,\ k = i = j \in [1, n] \tag{65}$$

Corollary 2 of Lemma 2. If ζ_k has been not less than ζ_k^* at the finite time $t = t_{\zeta_k}$, the initial state estimation covariance in the kth state direction has converged to a small enough magnitude, the kth state is considered convergent, and the magnitude of t_{ζ_k} indicates the observability degree of the nonlinear system in Eq. (45) (do not need to be proved).

4. Numerical simulations and analysis

To illustrate TAM-only attitude determination technique of the IRTSF for the spacecraft in the period of attitude changing, we undertake four numerical simulations with different scenarios. In the first two scenarios, it is assumed that the spacecraft is taking free spinning motion without any active attitude control. The difference of the first two scenarios is that, the spacecraft in the first scenario is initialized via a small angular velocity, and the spacecraft in the second scenario is initialized via a large angular velocity. In the last two scenarios, it is assumed that the spacecraft is taking the tumble motion with a constant angular velocity. To keep the spacecraft tumbling in a

Table 1
Initial state parameters with small angular velocity (for Scenarios 1 and 3).

Three attitude angles (roll, pitch, yaw), deg	Three-axis angular velocities, deg/s
15	0.2
10	0.1
15	0

constant angular velocity, an active control based on the reaction control system of spacecraft is implemented for the spacecraft. The difference of the first two scenarios is same with that described in the first two scenarios. Also, to directly perceive attitude determination simulation results of the spacecraft in the period of attitude changing, the results based on attitude quaternion will be transformed to Euler angles via Eq. (4). And all simulations are carried out with Matlab6.5 M-file programs and Simulink models.

4.1. Scenario 1: Spacecraft spinning motion with the small initial angular velocity and without any active attitude control

The initial attitude angles (denoted by Eulers) and small angular velocity of spacecraft are given in Table 1. The magnetic field vector is measured by the TAM, with a 10 s updating period and a standard deviation 50 nT for every axis, and the 10th-order EMF model (IGRF) is used as the EMF model. The IRTSF to estimate the attitude and angular is implemented by the discrete-time EKF in Eqs. (38)–(44), and all parameter propagations are based on the standard fourth-order Runge–Kutta method with a fixed step of 0.4 s. The IRTSF parameters are presented in Table 2. Also, the numerical simulations are performed by integrating the nonlinear attitude motion Eqs. (2) and (8) as the true attitude and angular velocity. Simultaneously, the rank of the observability matrix $\boldsymbol{M}_l$ with $l=2$, the condition number of the observability matrix $\boldsymbol{M}_{0/k}$, and the covariance matrix $P_{0/k}$ are calculated.

The rank of the observability matrix $\boldsymbol{M}_l$ equals seven all along in Fig. 3 which indicates the IRTSF for TAM-only attitude determination is locally weakly observable, and Fig. 4 shows that the condition number of observability matrix $\boldsymbol{M}_{0/k}$ varies between 0.8×10^7 and 4.3×10^7 (the same magnitude) in the course of simulation which indicates the observability degree of the IRTSF for TAM-only attitude determination is high. Fig. 5 shows the estimation errors of three attitude angles (Euler form) and three-axis angular velocities in body frame and the corresponding 3σ bounds. Obviously, three attitude angles in the body frame converge to the accuracy of less than 0.05° rapidly ($t<1$ h) and the corresponding 3σ bounds converge to less than 0.02° (see in Fig. 5). The angular velocity estimation error per axis in the body frame also converges to the accuracy of less than $2e-4^\circ$/s with the corresponding 3σ bounds less than $0.02\sim2e-4^\circ$/s rapidly (see in Fig. 5). The reasons for these results are attributed to the observability matrixes $\boldsymbol{M}_l$ and $\boldsymbol{M}_{0/k}$.

4.2. Scenario 2: Spacecraft spinning motion with the large initial angular velocity and without any active attitude control

The initial attitude angles (denoted by Eulers) and large angular velocity of spacecraft are given in Table 3.

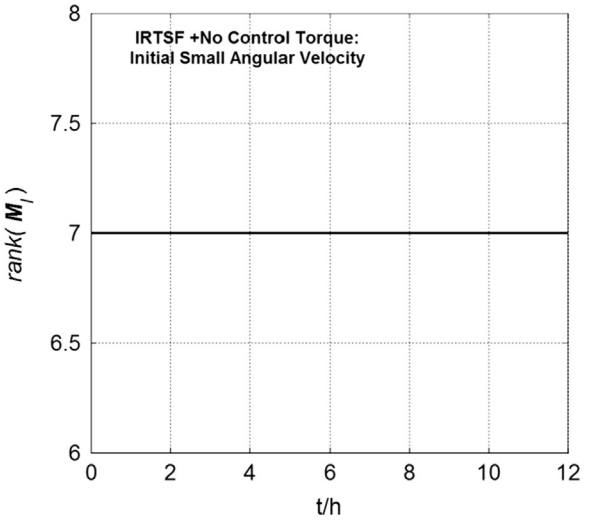

Fig. 3. Rank of the observability matrix, $\boldsymbol{M}_l$ (Scenario 1).

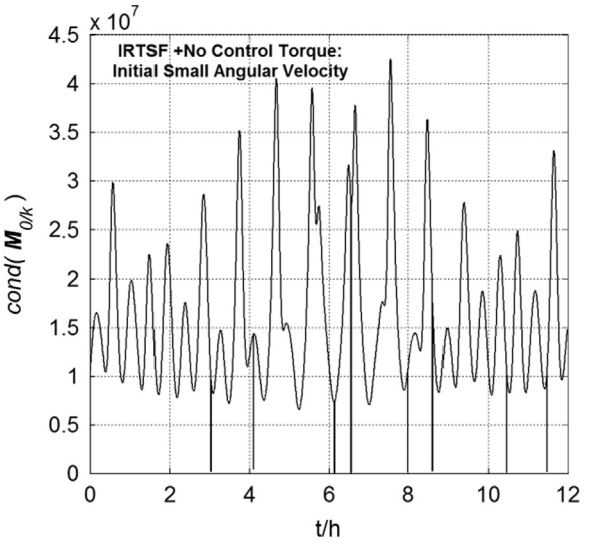

Fig. 4. Condition number of the observability matrix, $\boldsymbol{M}_{0/k}$ (Scenario 1).

Table 2
Simulation parameters of IRTSF (for all scenarios).

Parameters		Value
Standard deviations of process angular acceleration noises	$(\sigma_x, \sigma_y, \sigma_z)$, per axis, deg/s^2	0.0057
Standard deviations of TAM	$(\sigma_{bx},\sigma_{by},\sigma_{bz})$, per axis, nT	50
Measurement noises	$(\sigma_{\Delta bx},\sigma_{\Delta by},\sigma_{\Delta bz})$, per axis, nT	10
Standard deviations of initial attitude and angular velocity Estimation errors	Attitude angle, roll, pitch and yaw, deg Angular velocity, per axis, deg/s	2 0.1
Initial covariance matrix, $\boldsymbol{P}_0$	$\mathrm{Diag}\{\left[2^2;\ 2^2;\ 2^2;\ 0.1^2;\ 0.1^2;\ 0.1^2\right]\}\times(\pi/180)^2$	

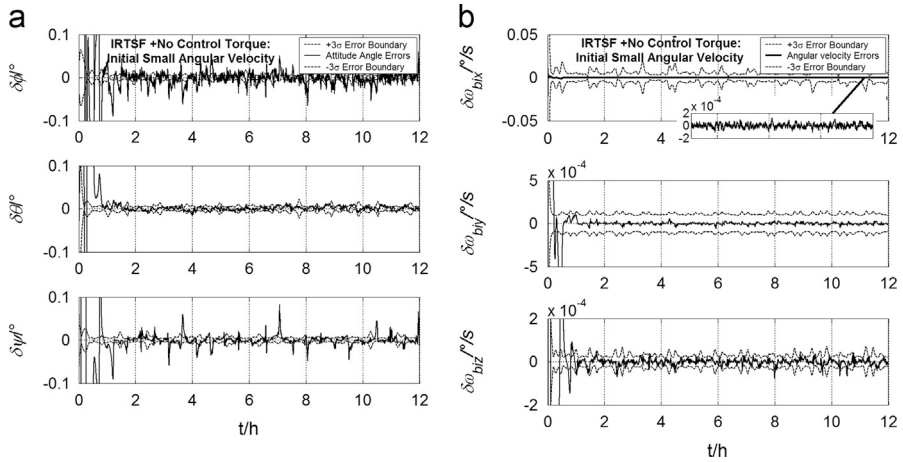

Fig. 5. State estimation errors in the body frame and corresponding 3σ bounds (Scenario 1). (a) Attitude angle estimation errors and (b) angular velocity estimation errors.

Table 3
Initial state parameters with Large angular velocity (for Scenarios 2 and 4).

Three attitude angles (roll, pitch, yaw), deg	Three-axis angular velocities, deg/s
15	2
10	1
15	0

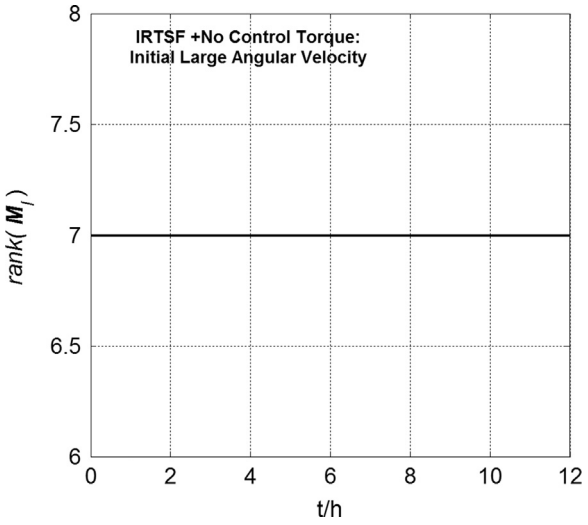

Fig. 6. Rank of the observability matrix, $\boldsymbol{M}_l$ (Scenario 2).

The IRTSF parameters are the same with Scenario 1 as are shown in Table 2.

The rank of the observability matrix $\boldsymbol{M}_l$ equals seven all along in Fig. 6 which indicates the IRTSF for TAM-only attitude determination is locally weakly observable, and Fig. 7 shows that the condition number of observability matrix $\boldsymbol{M}_{0/k}$ varies between 3×10^5 and 4.3×10^5 (the same magnitude) in the course of simulation which

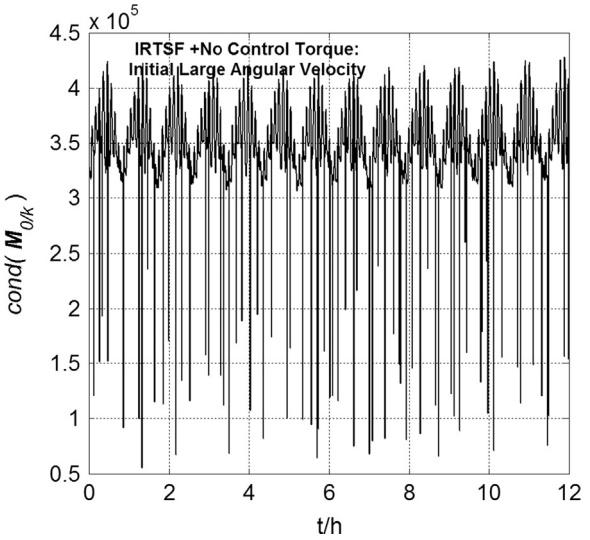

Fig. 7. Condition number of the observability matrix, $\boldsymbol{M}_{0/k}$ (Scenario 2).

indicates the observability degree of the IRTSF for TAM-only attitude determination is high. Compared the result in Fig. 7 with that in Fig. 4, the magnitude of the latter condition number is less, which indicates the observability degree of the IRTSF in the latter scenario is higher. Because the magnitude of the first derivation of the magnetic field vector in the latter scenario is larger to close the magnitude of the magnetic field vector, the capability of the IRTSF in the latter scenario is more strength to process large external perturbation. Of course, this result indicates that the IRTSF can be suitable for the TAM-only attitude determination with other serious initial angular velocity.

Fig. 8 shows the estimation errors of three attitude angles (Eulers) and three-axis angular velocities in body frame and the corresponding 3σ bounds. Obviously, three attitude angles in the body frame converge to the accuracy of less than 0.1° rapidly ($t<2$ h) and the corresponding 3σ bounds converge to less than 0.02° (see in Fig. 8). The angular velocity estimation error per axis in the body

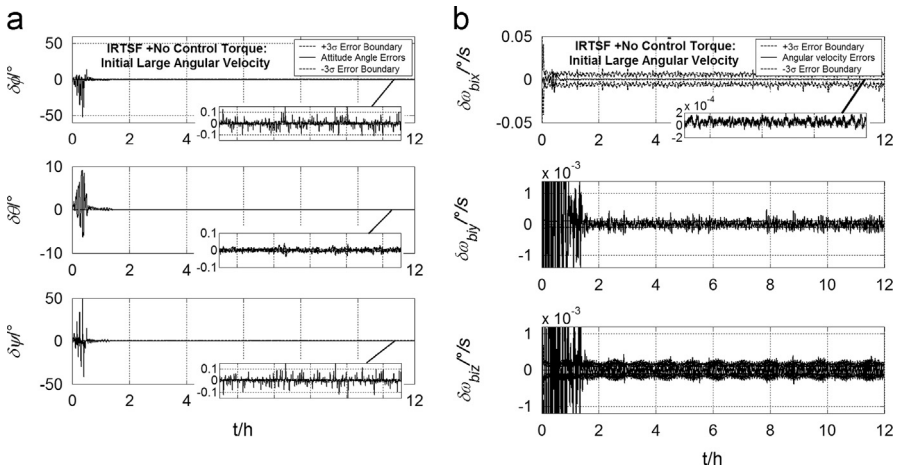

Fig. 8. State estimation errors in the body frame and corresponding 3σ bounds (Scenario 2). (a) Attitude angle estimation errors and (b) angular velocity estimation errors.

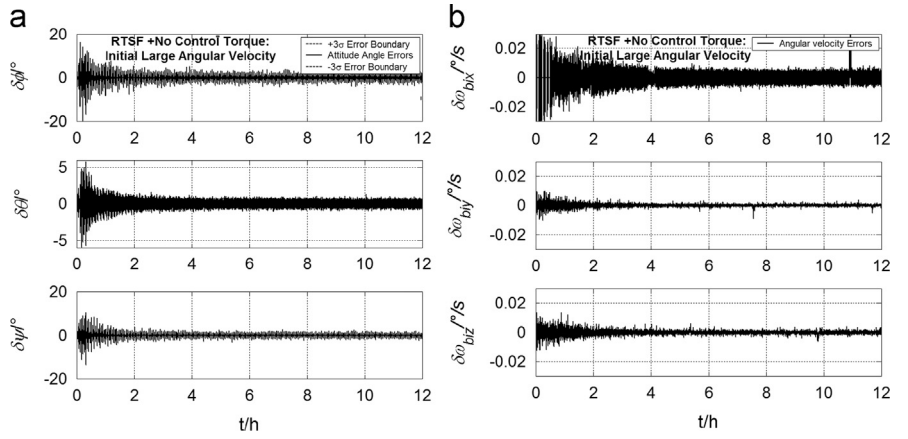

Fig. 9. State estimation errors based on RTSF in the body frame. (a) Attitude angle estimation errors and (b) angular velocity estimation errors.

frame also converges to the accuracy of less than $2e-4^\circ/s$ with the corresponding 3σ bounds less than $0.02\sim 2e-4^\circ/s$ rapidly (see in Fig. 8).

To acquire the advantage of the new TAM-only attitude determination method—IRTSF, a group simulation results of the traditional TAM-only attitude determination filter, that is RTSF, are shown in Fig. 9. Compared the results in Fig. 8 with those in Fig. 9, the attitude and angular velocity estimation accuracies of the IRTSF is higher to 1–2 order of magnitude, because there are the larger corrected errors of angular velocities in the RTSF as are shown in Fig. 9. Moreover, to evaluate the observability degrees of the IRTSF and RTSF, a group simulation results based on Eq. (65) is shown in Table 4. If the ζ_k^* is set to 90, the IRTSF is convergent at the finite time $t=2$, but the RTSF has not been convergent at the longer time $t=12$ (1 order of magnitude more). Therefore, the observability degree of the IRTSF is better than that of RTSF.

Also, to acquire the universality of the new TAM-only attitude determination method—IRTSF, the simulation results of the IRTSF with different initial attitude and angular velocity estimation errors for three axes are shown in Table 5. The simulation results indicates that, if the initial attitude angle estimation errors are close to the middle (between 70° and 110°), the state estimation errors of the IRTSF are in a large magnitude for the same initial angular velocity estimation errors, and with the increase of initial angular velocity estimation errors, the mentioned influence become more remarkable. Obviously, the estimation accuracy of the IRTSF can be guaranteed for any magnitude initial state estimation errors as are shown in Table 5, and the best and worst simulation results of the angular velocity estimations with the initial state estimation errors (30°, 1°/s) and (110°, 4°/s) for three axes in Table 5 are shown in Fig. 10.

Table 4
Observability degrees of IRTSF and RTSF.

Method	Simulation time (h)	ζ_k					
		$k=1$	$k=2$	$k=3$	$k=4$	$k=5$	$k=6$
IRTSF	2	99.5	99.1	98.3	99.9	99.7	99.9
RTSF	12	65.3	25.8	73.4	82	86	84

4.3. Scenario 3: Spacecraft tumble motion with the small initial angular velocity and an active attitude control

The initial attitude angles (denoted by Eulers) and small angular velocity of spacecraft are the same with Scenario 1 as are shown in Table 1. The IRTSF parameters are the same with Scenario 1 as are shown in Table 2.

The rank of the observability matrix $\boldsymbol{M}_l$ equals seven all along in Fig. 11 which indicates the IRTSF for TAM-only attitude determination is locally weakly observable, and Fig. 12 shows that the condition number of observability matrix $\boldsymbol{M}_{0/k}$ varies between 0.9×10^7 and 3×10^7 (the same magnitude) in the course of simulation which indicates the observability degree of the IRTSF for TAM-only attitude determination is high. Fig. 13 shows the estimation errors of three attitude angles (Euler form) and three-axis angular velocities in body frame and the corresponding 3σ bounds. Obviously, three attitude angles in the body frame converge to the accuracy of less than 0.05° rapidly ($t<1$ h) and the corresponding 3σ bounds

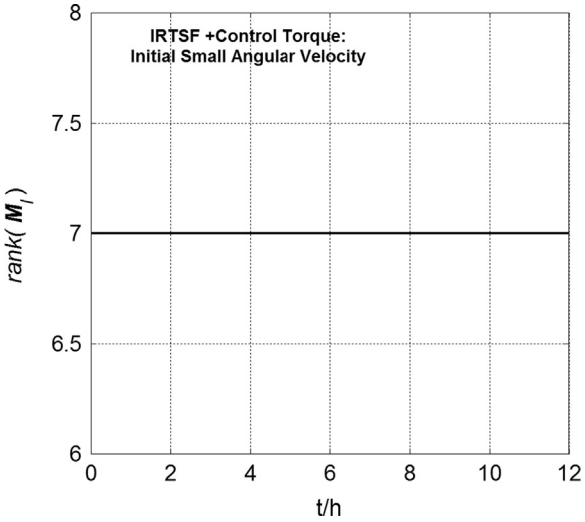

Fig. 11. Rank of the observability matrix, $\boldsymbol{M}_l$ (Scenario 3).

Table 5
Universality of IRTSF.

Initial attitude and angular velocity estimation errors for three axes	Estimation accuracy of IRSTF	
	Attitude angles (r.m.s)/deg	Angular velocity (r.m.s)/deg/s
(30°, 1°/s)	(0.0742,0.0349, 0.0671)	(0.0548, 0.1226, 0.1194)
(70°, 1°/s)	(0.0415, 0.0177, 0.0407)	(0.0331, 0.0988, 0.0953)
(110°, 1°/s)	(0.0419, 0.0179, 0.0411)	(0.0331, 0.0991, 0.0955)
(150°, 1°/s)	(0.0741, 0.0349, 0.0671)	(0.0547, 0.1225, 0.1193)
(30°, 2°/s)	(0.0737, 0.0347, 0.0666)	(0.0550, 0.1229, 0.1193)
(70°, 2°/s)	(0.1223, 0.0590, 0.1204)	(0.0410, 0.1456, 0.1414)
(110°, 2°/s)	(0.1244, 0.0601, 0.1225)	(0.0412, 0.1469, 0.1427)
(150°, 2°/s)	(0.0737, 0.0347, 0.0666)	(0.0549, 0.1228, 0.1192)
(30°, 3°/s)	(0.0894, 0.0419, 0.0806)	(0.0645, 0.1441, 0.1391)
(70°, 3°/s)	(0.2907, 0.1422, 0.2870)	(0.0608, 0.2638, 0.2597)
(110°, 3°/s)	(0.2943, 0.1445, 0.2915)	(0.0614, 0.2671, 0.2630)
(150°, 3°/s)	(0.0894, 0.0419, 0.0807)	(0.0645, 0.1440, 0.1391)
(30°, 4°/s)	(0.0159, 0.0065, 0.0163)	(0.0361, 0.0692, 0.0695)
(70°, 4°/s)	(0.4771, 0.2337, 0.4732)	(0.0834, 0.4020, 0.3986)
(110°, 4°/s)	(0.4835, 0.2367, 0.4794)	(0.0842, 0.4066, 0.4033)
(150°, 4°/s)	(0.0159, 0.0065, 0.0163)	(0.0361, 0.0692, 0.0695)

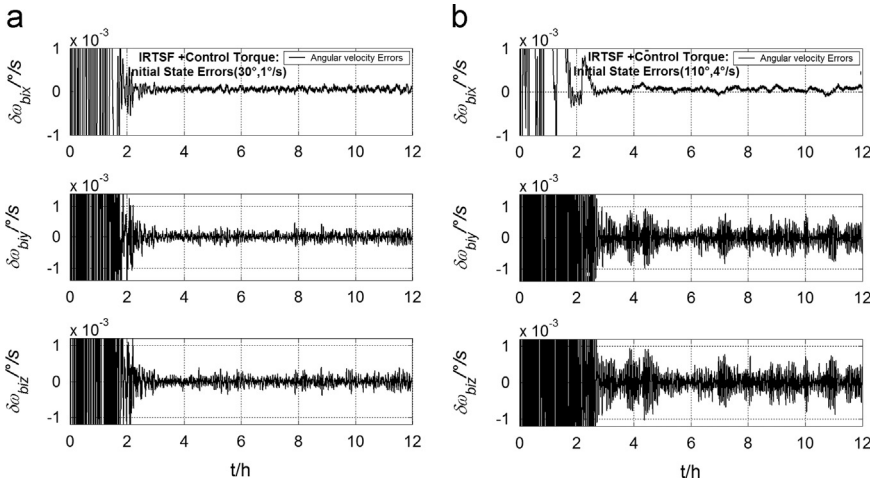

Fig. 10. Angular velocity estimation errors with different initial state estimation errors in the body frame. (a) Angular velocity estimation errors and (b) angular velocity estimation errors.

converge to less than 0.04° (see in Fig. 13). The angular velocity estimation error per axis in the body frame also converges to the accuracy of less than $2e-4^\circ/s$ with the corresponding 3σ bounds less than $0.02\sim 2e-4^\circ/s$ rapidly (see in Fig. 13). Compared the results in Fig. 13 with that in Fig. 5, the estimation accuracies of the attitude angles and the angular velocities are basically accordant, which indicates the IRTSF is still reliable and firm for an active control, and the related conclusion is different from that of RTSF [14].

4.4. Scenario 4: Spacecraft tumble motion with the large initial angular velocity and an active attitude control

The initial attitude angles (denoted by Eulers) and small angular velocity of spacecraft are the same with the Scenario 2 as are shown in Table 3. The IRTSF parameters are the same with Scenario 1 as are shown in Table 2.

The rank of the observability matrix $\boldsymbol{M}_l$ equals seven all along in Fig. 14 which indicates the IRTSF for TAM-only attitude determination is locally weakly observable, and Fig. 15 shows that the condition number of observability matrix $\boldsymbol{M}_{0/k}$ varies between 3.2×10^5 and 4.2×10^5 (the same magnitude) in the course of simulation which indicates the observability degree of the IRTSF for TAM-only attitude determination is high. Fig. 16 shows the estimation errors of three attitude angles (Euler form) and three-axis angular velocities in body frame and the corresponding 3σ bounds. Obviously, three attitude angles in the body frame converge to the accuracy of less than 0.02° rapidly ($t<1$ h) and the corresponding 3σ bounds converge to less than 0.01° (see in Fig. 16). The angular velocity estimation error per axis in the body frame also converges to the accuracy of less than $2e-4^\circ/s$ with the corresponding 3σ bounds less than $0.02\sim 2e-4^\circ/s$ rapidly (see in Fig. 16). Compared the results in Fig. 16 with that in

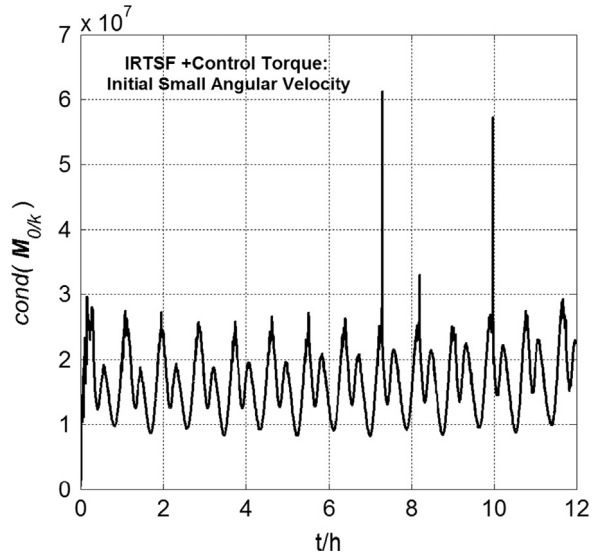

Fig. 12. Condition number of the observability matrix, $\boldsymbol{M}_{0/k}$ (Scenario 3).

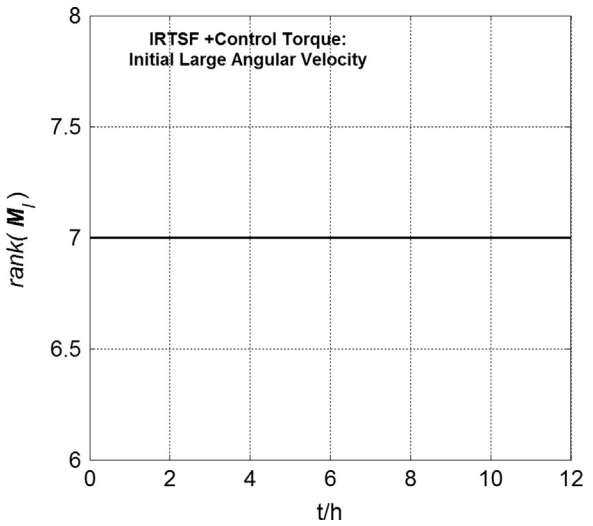

Fig. 14. Rank of observability matrix, $\boldsymbol{M}_l$ (Scenario 4).

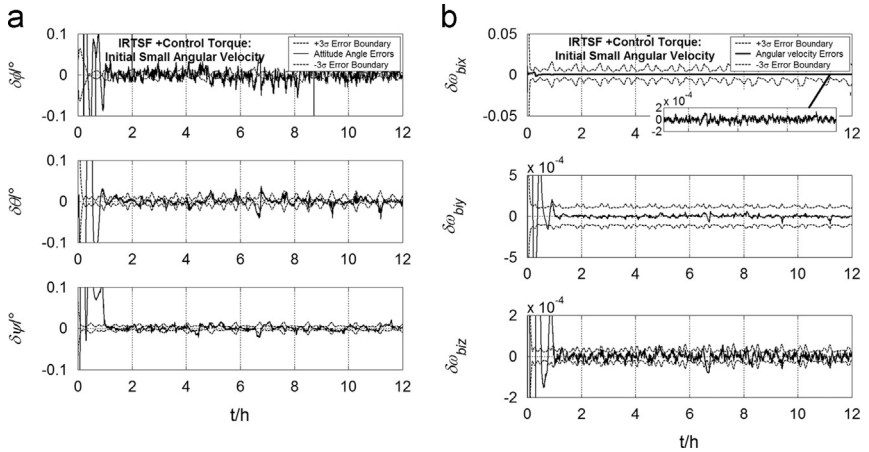

Fig. 13. State estimation errors in the body frame and corresponding 3σ bounds (Scenario 3). (a) Attitude angle estimation errors and (b) angular velocity estimation errors.

Fig. 8, the estimation accuracies of the attitude angles and the angular velocities are basically accordant, which indicates the IRTSF with the large initial angular velocity is also reliable and firm for an active control.

5. Conclusions

Some past research works have illustrated that the attitude determination technology of only three-axis magnetometer (TAM) is feasible for spacecraft running in the period of attitude changing (fast and large angular attitude maneuver, rapidly spinning or uncontrolled tumble). However, due to the corrected bias of angular velocity, the attitude determination accuracies of those methods, such as the deterministic magnetometer-only attitude and rate determination (DADMOD) and the real-time sequential filter (RTSF), are insufficient. Therefore, an improved TAM-only attitude determination technique—IRTSF is presented in this paper. In this improved method, the attitude dynamic equation is directly leaded into the process noise model of the IRTSF, and the angular velocity is directly corrected to guarantee the state estimation accuracy, especially the estimation accuracy of angular velocity, by the angular velocity information of first order derivation measurement. A discrete-time extended Kalman filter (EKF) is developed to estimate the attitude angles and angular velocities of spinning spacecraft and tumble spacecraft with small and large initial angular velocities. The Lie-Differentiation is utilized to analyze the local observability of the improved TAM-only attitude determination system. The observability degree of the improved TAM-only attitude determination system—IRTSF is evaluated by the condition number, and is compared with that of RTSF by a solved covariance matrix. The improved TAM-only attitude determination method is verified by numerical simulations. The results indicate that (1) the attitude angle and angular velocity estimation systems of spinning spacecraft and tumble spacecraft with small or large initial angular velocities based on the IRTSF are all observable, and their estimation accuracies are sufficient and better than those of the RTSF, (2) compared the observability degrees of the IRTSF and the RTSF, the IRTSF can be convergent to sufficient accuracy at a finite (short enough) time, (3) usually, the initial state of the RTSF for TAM-only attitude estimation need to be determined by the DADMOD method, but the initial condition of the IRTSF can be fuzzy, and the convergence and universality of the IRTSF can be guaranteed for any large enough initial state estimation errors, and (4) different from the attitude estimation results of the RTSF, those of the IRTSF is not influenced by the active control torque. Therefore, the IRTSF is a reliable, firm and universal TAM-only attitude estimation method with sufficient accuracy.

Also, because the TAM is assumed as a dream sensor with white Gaussian noises, the scale factors and the nonorthogonality of TAM are not discussed for the improved TAM-only attitude determination method—IRTSF. Therefore, the future work will focus on the accuracy and observability influence of the earth magnetic field

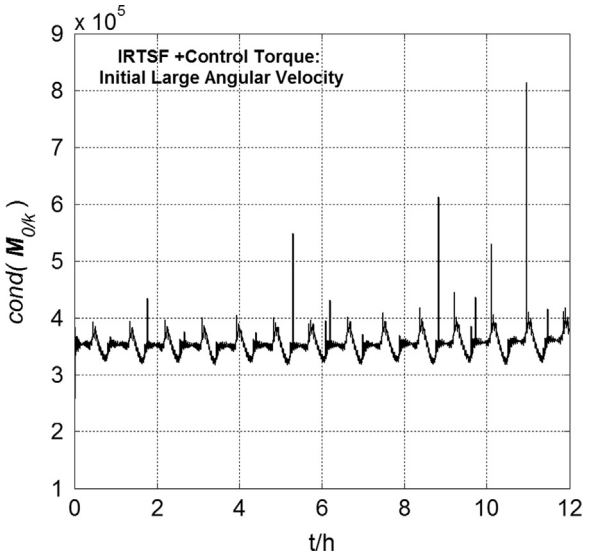

Fig. 15. Condition number of observability matrix, $\boldsymbol{M}_{0/k}$ (Scenario 4).

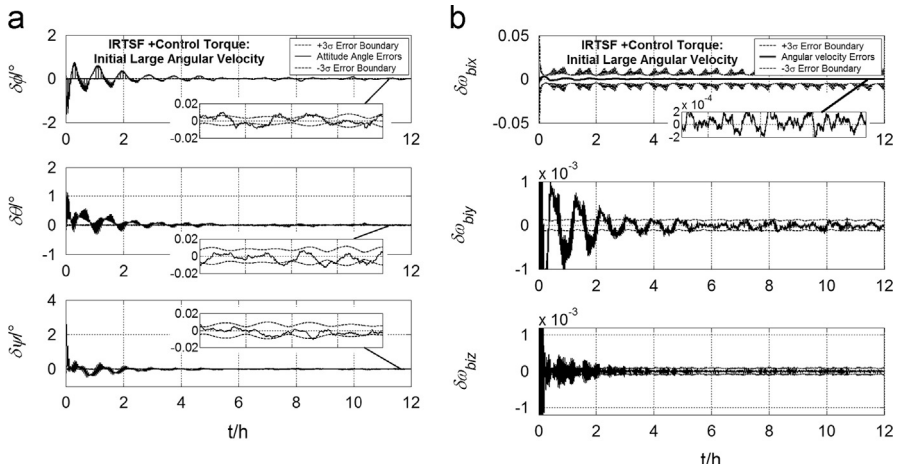

Fig. 16. State estimation errors in the body frame and corresponding 3σ bounds (Scenario 4). (a) Attitude angle estimation errors and (b) angular velocity estimation errors.

(EMF) model uncertainties and the scale factors and nonorthogonality of TAM on the IRTSF TAM-only attitude determination method.

Acknowledgments

The paper is supported by the National Natural Science Foundation of China (Ref. 11272028). The authors thank the associate editor and the reviewers for their helpful suggestion and revision to improve this paper.

Reference

[1] F. Xing, et al., APS star tracker and its attitude estimation, in: 1st IEEE International Symposium on Systems and Control in Aerospace and Astronautics, Harbin, Republic of China, January 2006, pp. 34–38.
[2] P. Ortega, et al., A miniaturized two axis sun sensor for attitude control of Nano-satellites, IEEE Sens. J. 10 (10) (2010) 1623–1632.
[3] H. Kim, et al., Design concept for autonomous operation of KITSAT-3, an experimental LEO microsatellite, in: Aerospace Conference Proceedings, 2000 IEEE, Big Sky, MT, vol. 2, March 2000, pp. 459–465.
[4] A.M.S. Mohammed,et al., Alsat-1 first algerian low earth orbit observation microsatellite in orbit, in: IEEE Information and Communication Technologies, Damascus, vol. 2, 2006, pp. 2518–2523.
[5] T. Kuwahara, et al., Satellite-to-ground optical communication system on low earth orbit micro-satellite RISESAT, in: 2012 IEEE/SICE International Symposium on System Integration, Fukuoka, December 2012, pp. 939–944.
[6] A. Grosz, et al., A three-axial search coil magnetometer optimized for small size, low power, and low frequencies, IEEE Sens. J. 11 (4) (2011) 1088–1094.
[7] M.L. Battagliere, et al., Passive magnetic attitude stabilization system of the EduSAT microsatellite, J. Aerosp. Eng. 224 (2010) 1097–1106.
[8] M.L. Psiaki, F. Martel, P.K. Pal, Three-axis attitude determination via Kalman filtering of magnetometer data, J. Guidance Control Dyn. 13 (3) (1989) 506–514.
[9] T.E. Humphreys, et al., Magnetometer-based attitude and rate estimation for spacecraft with wire booms, J. Guidance Control Dyn. 28 (4) (2005) 584–593.
[10] J. Cote, J. Lafontaine, Magnetic-only orbit and attitude estimation using the square-root unscented Kalman filter: application to the PROBA-2 spacecraft, in: AIAA Guidance, Navigation and Control Conference and Exhibit, Hawaii, August 2008, pp. 1–24.
[11] C.S. Hart, Satellite attitude determination using magnetometer data only, in: 47th AIAA Aerospace Sciences Meeting, Orlando, Florida, January 2009, pp. 1–11.
[12] J.L. Crassidis, F.L. Markley, Predictive filtering for attitude estimation without rate sensors, J. Guidance Control Dyn. 20 (3) (1997) 522–527.
[13] G. Natanson, S. McLaughlin, R. Nicklas, A method of determining attitude from magnetometer data only, in: Proceedings of the Flight Mechanics/Estimation Theory Symposium 1990, Greenbelt, May 1990, pp. 359–378.
[14] M. Challa, S. Kotaru, G. Natanson, Magnetometer-only attitude and rate estimates during the earth radiation budget satellite 1987 control anomaly, in: Proceedings of the AIAA Guidance, Navigation, and Control, vol. 2, 1997, pp. 830–840.
[15] M. Challa, G. Natanson, et al., Advantages of estimating rate corrections during dynamic propagation of spacecraft rates—applications to real-time attitude determination of SAMPEX, in: Proceedings of the Flight Mechanics/Estimation Theory Symposium 1994, Greenbelt, May 1994, pp. 481–495.
[16] M. Challa, G. Natanson, N. Ottenstein, Magnetometer-only attitude and rate estimates for spinning spacecraft, in: Proceedings of the AIAA/AAS Astrodynamics Specialists Conference, Denver, 2000, pp. 311–321.
[17] M.D. Shuster, S.D. Oh, Three-axis attitude determination from vector observations, J. Guidance Control Dyn. 4 (1) (1981) 70–77.
[18] R. Hermann, A.K. Krener, Nonlinear controllability and observability, IEEE Trans. Autom. Control AC-22 (5) (1977) 728–740.
[19] G.E. Forsythe, M.A. Malcolm, C.B. Moler, Computer Methods for Mathematical Computations, Prentice-Hall, Englewood Cliffs, NJ, 1977, 47.
[20] S. Hong, H.H. Chun, Singular value decomposition approach to observability analysis of GPS/INS, in: Proceedings pf the IAIN/GNSS, Jeju, Korea, October 2006, pp. 133–138.
[21] G.S. Mohinder, P.A. Angus, Kalman Filtering: Theory and Practice Using MATLAB, Second ed. John Wiley & Sons, Inc., New York, 2001, 178–181.
[22] A. Gelb, J.F. Kasper, R.A. Nash, C.F. Price, A.A. Sutherland, Applied Optimal Estimation, MIT Press, Cambridge, MA, 1974, 107–113.
[23] J.L. Crassidis, J.L. Junkins, Optimal Estimation of Dynamic Systems, Chapman and Hall CRC, New York, 2004(Chapter 7).
[24] F.L. Markley, Autonomous navigation using landmark and intersatellite data, in: AIAA/AAS Astrodynamics Conference, Seattle, WA, 1984, AIAA, pp. 1984–1987.